Orientational Disorder, the Orientational Density Distribution and the Rotational Potential in C$_{60}$

P. Schiebel,[a] K. Wulf,[a] W. Prandl,[a] G. Heger,[b] R. Papoular[c] and W. Paulus[c]

[a]*Institut für Kristallographie, Universität Tübingen, Charlottenstrasse 33, D-72070 Tübingen, Germany,* [b]*Institut für Kristallographie, RWTH-Aachen, Templergraben 55, D-52062 Aachen, Germany, and* [c]*Laboratoire Léon Brillouin, C E de Saclay, F-91191 Gif-sur-Yvette, France*

Abstract

Bragg intensities from neutron and X-ray diffraction data of C$_{60}$ single crystals were used to determine the nuclear- and electron-density distributions of C$_{60}$ at room temperature. The anisotropic density distribution is reconstructed by the maximum-entropy method and evaluated in terms of symmetry-adapted spherical harmonics. From this analysis, the orientational probability density function $f(\omega)$ has been calculated and the rotational potential $V(\omega)$ that is experienced by a C$_{60}$ molecule in the cubic surrounding at 295 K has been obtained. $f(\omega)$ shows strong deviations from the uniform orientational probability density function that would result from isotropic rotation. Accordingly, $V(\omega)$ exhibits well developed minima. The absolute potential minimum is found at an Euler-angle set ω_1 and a second set of minima at slightly higher energy at ω_2. The potential difference between $V(\omega_1)$ and $V(\omega_2)$ is 313 K, whereas the overall rotational potential barrier height amounts to 522 K. ω_1 and ω_2 are comparable with the major and minor orientations that are adopted by the molecules in their low-temperature arrangement. The angles ω_1 and ω_2 are fixed by the intrinsic geometry of the Euler-angle space (α, β, γ) under the combined action of the cubic site and the icosahedral molecular point group.

1. Introduction

Being the prototype of the large family of fullerenes (Krätschmer, Lamb, Fostiropoulus & Huffman, 1990), C$_{60}$ has attracted interest in recent years due to its extremely high symmetry and its structural, dynamical and thermodynamic properties.

The first clear evidence that C$_{60}$ exhibits full icosahedral symmetry came from nuclear magnetic resonance experiments (Johnson, Yanonni, Dorn, Salem & Bethune, 1992), which gave a single sharp resonance line, consistent with only one type of chemical site for all C atoms in this molecule (Fig. 1). As a result, the C$_{60}$ molecule forms a regular truncated icosahedron consisting of 20 hexagonal and 12 additional pentagonal faces to form a closed shell. Although all C atoms

are equivalent, they are held together by two different types of bonds. Two of the three bonds of every C atom are electron-poor single bonds, the third is an electron-rich double bond. The single bonds form regular pentagons, whereas the hexagons are built up by alternating single and double bonds, whose lengths d_1 and d_2 are approximately 1.45 and 1.40 Å, respectively (Leclerq *et al.*, 1993). The diameter of the C$_{60}$ molecule is 7.1 Å if one regards the centre-of-mass positions of the C atoms, but taking account of the size of the π-electron orbitals associated with each C atom, the outer diameter of the C$_{60}$ molecule, *i.e.* the distance between next-nearest neighbours, is 10.02 Å (Krätschmer, Lamb, Fostiropoulus & Huffman, 1990).

In the solid state, the C$_{60}$ molecules crystallize at room temperature in a cubic face-centred structure ($Fm\bar{3}m$) with a lattice constant of 14.17 Å, where all molecules are structurally equivalent. Dynamically, they undergo three-dimensional rotations and early X-ray powder diffraction data indicated that, to a good approximation, these molecules can be considered as spinning freely, assuming that every molecule adopts
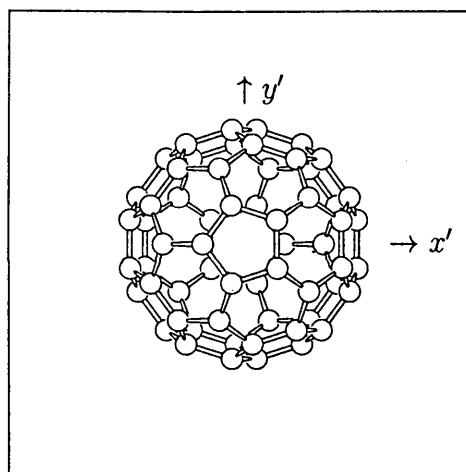

Fig. 1. The C$_{60}$ molecule viewed along one of its molecular fivefold axes. x' and y' denote the coordinate system fixed in the molecule; z' is out of the plane of the paper.

any orientation with equal probability (Heiney, 1992; Heiney *et al.*, 1991; Sachidanandam & Harris, 1991; Copley, Neumann, Cappelletti, Kamitakahara, Prince *et al.*, 1992).

Yet neutron scattering and NMR data indicate a hindered rotation at room temperature. The reorientational time was found to be 0.9×10^{-11} s at 300 K, about a factor of three slower than for unhindered rotation and almost 50% faster than in solution (Neumann *et al.*, 1991; Copley, Neumann, Cappelletti & Kamitakahara, 1992; Johnson, Yanonni, Dorn, Salem & Bethune, 1992).

Obviously, the assumption of completely random orientation is an oversimplification, since C_{60} molecules do not have spherical symmetry and the interaction between molecules depends to some extent on their mutual orientation. Chow *et al.* (1992) were the first to demonstrate the nonuniform room-temperature electron-density distribution from X-ray synchrotron diffraction, which was confirmed recently by neutron diffraction (David, Ibberson & Matsuo, 1993; Papoular, Roth, Heger, Haluska & Kuzmany, 1993).

On cooling, C_{60} shows two anomalies in the thermal expansion (Gugenberger *et al.*, 1992) at $T_1 = 261$ K and at $T_2 \simeq 90$ K. The anomaly at 261 K is a first-order phase transition from the f.c.c. ($Fm\bar{3}m$) into a primitive ($Pa\bar{3}$) lattice (Heiney *et al.*, 1991; David, Ibberson, Dennis, Hare & Prassides, 1992a), which was at first interpreted as a transition from three-dimensional to uniaxial rotation. In the meantime, it is known that there remains appreciable three-dimensional disorder below T_1 (Bürgi *et al.*, 1992; Michel, Lamoen & David, 1995). At $T_2 \simeq 90$ K, a glass transition occurs (Gugenberger *et al.*, 1992).

The dynamics in the $Pa\bar{3}$ structure are now described by reorientations between two energetically slightly different sets of symmetry-equivalent orientations (David, Ibberson, Dennis, Hare & Prassides, 1992a,b). In one of them, an electron-rich double bond of one C_{60} molecule is aligned opposite to an electron-poor pentagonal face. This orientation was identified as the most probable orientation at 10 K by David *et al.* (1991). In the other one, with only slightly higher energy, the electron-rich double bond of one C_{60} molecule is placed opposite to an electron-poor hexagonal face. This orientation is obtained from the lower-energy orientation by rotation of the C_{60} molecule by 60° around a $\langle 111 \rangle$ axis. At 250K, ~60% of the molecules are found in the 'pentagon facing' and ~40% in the 'hexagon facing' orientation.

The reorientational motion described above allows a greater fraction of C_{60} molecules to align in the lower-energy configuration, *i.e.* pentagons facing double bonds, as the temperature is decreased. By $T = 90$ K, ~83% of the intermolecular alignments are reported to be in the lower-energy state, leaving ~17% in the higher-energy state. Below 90 K, the same fraction of the relative intermolecular orientations is maintained (David, Ibberson, Dennis, Hare & Prassides, 1992b).

The single-particle rotational potential introduced by James & Keenan (1959) in their seminal paper on orientational disorder of methane and later determined for small molecules from neutron diffraction data (Vogt & Prandl, 1983; Gerlach, Prandl & Vogt, 1984; Hoser, Joswig, Prandl & Vogt, 1985) has been introduced and worked out for C_{60} in a series of theoretical papers covering many aspects of the high- and low-temperature phases (Michel, 1992a,b; Michel, Copley & Neumann, 1992; Heid, 1993; Copley & Michel, 1993; Lamoen & Michel, 1994; Michel, Lamoen & David, 1995). A comprehensive review on structure and dynamics of C_{60} has been given recently by Axe, Moss & Neumann (1994).

The purpose of the present paper is to derive the single-particle hindrance potential for the high-temperature phase ($Fm\bar{3}m$) strictly from experimental data without any *a priori* assumptions as to, for example, its absolute magnitude. The electron-density distribution is obtained from X-ray diffraction experiments, whereas the nuclear-density distribution is found from neutron diffraction. Since these two densities are physically not equivalent, a combined neutron and X-ray study is required to distinguish between chemical bonding effects and atomic distributions, *i.e.* preferred orientations of C_{60} molecules.

The paper is organized as follows. §2 describes the neutron and X-ray experiments at room temperature. In §3, a review of the theoretical concepts leading to the orientational probability density function and the rotational potential is given. In §4.1, we use two distinct procedures, leading to the same qualitative picture: an anisotropic density distribution of the C_{60} molecules. In §§4.2 and 4.3, we obtain the orientational probability density distribution and the rotational potential for C_{60}. Consequences for the orientational dynamics are discussed in §5.

2. Experimental and crystal parameters

The three C_{60} crystals used in our room-temperature study were grown by sublimation (Haluska, Kuzmany, Vybornov, Rogl & Fejdi, 1993). Our C_{60} crystal for the X-ray experiment was isometrical ($d = 0.2$ mm) and showed no detectable twins. The cubic lattice parameter was refined to 14.152 (2) Å. A conventional 4-circle Stoe diffractometer, equipped with a graphite (002) monochromator, was operated at a wavelength $\lambda_{\text{Mo } K\alpha} = 0.71073$ Å. Using $\omega - 2\theta$ scans, 1894 Bragg intensities were collected up to $\sin\theta/\lambda = 0.65$ Å^{-1}. They resulted in 205 unique reflections with an internal agreement factor $R_{\text{int}} = 0.039$.

Two neutron experiments were performed at the four-circle diffractometer 5C2 at the hot source of the Orphee reactor with a neutron wavelength of $\lambda = 0.8308$ (2) Å selected by a Cu(220) vertically focusing monochroma-

tor and a 0.25 mm thick erbium filter to reduce $\lambda/2$ contamination to less than 0.1%.*

Our first crystal was about 3 mm^3 in volume and showed natural (100) and (111) faces. Two sizable twins were detected, originating from stacking faults along different [111] directions. Together with the main domain of our sample, they correspond to a volume contribution of 9.3, 2.3 and 88.4%, respectively. In the second crystal (2.8 mm^3), with only one detectable twin, 95% of the volume contributed to the main domain.

The experiments were performed in such a way that only those 'pure' Bragg reflections of the main domain orientation were registered that were unaffected by the contribution from the minor twins.

In the first data set, 210 non-twin-affected Bragg intensities were measured, using ω scans up to $\sin\theta/\lambda = 0.51$ Å^{-1}, and in this way 102 unique reflections ($R_{int} = 0.022$) were obtained. In the second data set, 478 Bragg intensities up to $\sin\theta/\lambda = 0.78$ Å^{-1} were collected, resulting in 342 unique reflections ($R_{int} = 0.019$).

Absorption effects are negligible in all three data sets (X-ray: $\mu R < 0.005$; neutron: $\mu R < 0.0001$). A correction factor c_{ext} was included in the data analysis (§4.1) to account for secondary extinction.

3. Theory

The structure factor of a rotationally disordered molecular crystal is basically derived from the Fourier transform of the molecular scattering amplitude. This amplitude is at first (Press & Hüller, 1973; Prandl, 1981) expressed in a molecular frame Σ' rigidly connected with the molecule in terms of symmetry-adapted spherical harmonic functions (SAF's) $\Pi_{l\varepsilon'}(\hat{r}')$. In the next step, this amplitude must be transformed into the crystal frame Σ and be expressed in terms of SAF's $P_{l\varepsilon}(\hat{r})$ having the symmetry of the site occupied by the molecule. The third step consists of averaging these amplitude contributions with the orientational probability function $f(\omega) \equiv f(\alpha, \beta, \gamma)$ with the Euler angles (α, β, γ).

We use $\mathbf{r} = (r, \theta_r, \varphi_r)$, $\mathbf{Q} = (q, \theta_Q, \varphi_Q)$ together with the corresponding primed symbols $\mathbf{r}'$, $\mathbf{Q}'$ referring to Σ' and unit vectors $\hat{r}$, $\hat{r}'$, $\hat{Q}$, $\hat{Q}'$ in order to indicate unequivocally the angular variables θ_r, φ_r etc. in $Y_{lm}(\hat{r})$, $\Pi_{l\varepsilon'}(\hat{r}')$ and $P_{l\varepsilon}(\hat{r})$.

3.1. Definitions

The totally symmetric symmetry-adapted functions $P_{l\varepsilon}(\hat{r})$ of the point group of the lattice site of the centre of mass of the C_{60} molecule ($m\bar{3}m$) are given by

$$P_{l\varepsilon}(\hat{r}) = \sum_{m=-l}^{l} Y_{lm}(\hat{r})P_{m\varepsilon}^{l} \tag{1}$$

and the SAF's $\Pi_{l\varepsilon'}$ of the icosahedral point group of the C_{60} molecule by

$$\Pi_{l\varepsilon'}(\hat{r}') = \sum_{m'=-l}^{l} Y_{lm'}(\hat{r}')\Pi_{m'\varepsilon'}^{l}. \tag{2}$$

The origins of both systems Σ and Σ' coincide, so r and r' are identical. ε and ε' enumerate the different SAF's for given l. Coefficients $P_{m\varepsilon}^{l}$ for the cubic point group can be found in Bradley & Cracknell (1972) and Müller & Priestley (1966). Analytical expressions for the icosahedral SAF's with $l = 6$ and $l = 10$ are given by Cohan (1958). High-order SAF's for $l \le 30$ have been determined by a recursive algorithm by Prandl, Schiebel & Wulf (1996).

To transform one kind of SAF into the other, the mixed rotator functions $\mathcal{M}$ are used (Prandl, 1981):

$$\Pi_{l\varepsilon'}(\hat{r}') = \sum_{\varepsilon} P_{l\varepsilon}(\hat{r})\mathcal{M}_{\varepsilon\varepsilon'}^{l}(\omega), \tag{3}$$

where $\omega = (\alpha, \beta, \gamma)$ is the set of Euler angles that transforms the unprimed system into the primed system. The mixed rotator functions are given by

$$\mathcal{M}_{\varepsilon\varepsilon'}^{l}(\omega) = \sum_{m,m'=-l}^{l} \mathcal{D}_{mm'}^{l}(\omega)P_{m\varepsilon}^{*l}\Pi_{m'\varepsilon'}^{l}. \tag{4}$$

The $\mathcal{D}_{mm'}^{l}(\omega)$ are the Wigner functions, which describe the rotation of spherical harmonics (Wigner, 1959). The mixed rotator functions satisfy the orthonormality relation:

$$\int \mathcal{M}_{\varepsilon_1\varepsilon_1'}^{*l_1}\mathcal{M}_{\varepsilon_2\varepsilon_2'}^{l_2} d\omega = [8\pi^2/(2l_1+1)]\delta_{l_1,l_2}\delta_{\varepsilon_1,\varepsilon_2}\delta_{\varepsilon_1',\varepsilon_2'}. \tag{5}$$

3.2. Method

The coherent scattering structure factor of the unit cell is given by

$$F(\mathbf{Q}) = \exp(i\mathbf{Q} \cdot \mathbf{r}^0)T(\mathbf{Q})F^{rot}(\mathbf{Q}). \tag{6}$$

Here, $\mathbf{Q} = 2\pi\mathbf{H}$ is the momentum transfer, $\mathbf{r}^0$ the equilibrium position of the centre of mass of a rigid C_{60} molecule, $T(\mathbf{Q})$ the translational part of the scattering factor, normally a Debye–Waller factor, and $F^{rot}(\mathbf{Q})$ the rotational part. This separation of the translational and rotational parts of the structure factor is only valid if the translational and rotational parts of the molecular motion are not correlated (Press & Hüller, 1973). The rotational structure factor is given by

$$F^{rot}(\mathbf{Q}) = \int_{cell} \exp(i\mathbf{Q} \cdot \mathbf{r})a(\mathbf{r}) d\mathbf{r} = a(\mathbf{Q}). \tag{7}$$

To calculate the rotational potential of the C_{60} molecule, consider first the form factor in the molecule-fixed

coordinate system Σ':

$$b(\mathbf{Q}') = \sum_i \exp(i\mathbf{Q}' \cdot \mathbf{r}_i') f_{X,N}(\mathbf{Q}'), \qquad (8)$$

where $f_{X,N}(\mathbf{Q})$ is the X-ray form factor or the neutron scattering length. By expanding $\exp(i\mathbf{Q}' \cdot \mathbf{r}_i')$ through the SAF's of the icosahedral group $\Pi_{l\varepsilon'}(\theta', \varphi')$, one gets

$$b(\mathbf{Q}') = 4\pi f_{X,N}(\mathbf{Q}') \sum_i \sum_{l\varepsilon'} i^l j_l(Q'r_m') \Pi_{l,\varepsilon'}(\hat{\mathbf{r}}_i') \Pi_{l,\varepsilon'}(\hat{\mathbf{Q}}'), \qquad (9)$$

where r_m is the radius of the C_{60} molecule. This expansion can be transformed into the crystal-fixed coordinate system Σ by using the transformation properties of the SAF's [(3)]. We get

$$b(\mathbf{Q}) = 4\pi f_{X,N}(\mathbf{Q}) \sum_{l\varepsilon'} i^l j_l(Qr_m) \overline{\Pi}_{l\varepsilon'} \sum_\varepsilon P_{l\varepsilon}(\hat{\mathbf{Q}}') \mathcal{M}_{\varepsilon\varepsilon'}^l(\omega) \qquad (10)$$

with the structure constants (Prandl, 1981) of the disordered molecule:

$$\overline{\Pi}_{l\varepsilon'} = \sum_i \Pi_{l\varepsilon'}(\hat{\mathbf{r}}_i). \qquad (11)$$

The averaged form factor $a(\mathbf{Q})$ can be calculated from $b(\mathbf{Q})$ by introducing a probability function $f(\omega)$ for the orientation of the molecular frame Σ' with respect to the crystal frame Σ (Press & Hüller, 1973):

$$a(\mathbf{Q}) = \int f(\omega) b(\mathbf{Q}) \, d\omega. \qquad (12)$$

Expanding $f(\omega)$ into the mixed rotator functions:

$$f(\omega) = \sum_{l\varepsilon\varepsilon'} g_{\varepsilon\varepsilon'}^l \mathcal{M}_{\varepsilon\varepsilon'}^l(\omega) \qquad (13)$$

and combining this with (5) and (12), we find an expansion of the averaged molecular form factor $a(\mathbf{Q})$:

$$a(\mathbf{Q}) = 4\pi f_{X,N}(\mathbf{Q}) \sum_{l\varepsilon} i^l j_l(Qr_m)$$
$$\times [8\pi^2/(2l+1)] \sum_{\varepsilon'} g_{\varepsilon\varepsilon'}^l \overline{\Pi}_{l\varepsilon'} P_{l\varepsilon}(\hat{\mathbf{Q}}). \qquad (14)$$

Alternatively, the scattering-length density $a(\mathbf{r})$ can be expressed as a convolution of the electron or nuclear density of the C atoms $\rho_{El}(\mathbf{r})$ or $\rho_N(\mathbf{r})$, respectively, and a number density for the centres of the C atoms $W(\mathbf{r})$:

$$a(\mathbf{r}) = W(\mathbf{r}) * \rho_{El,N}(\mathbf{r}). \qquad (15)$$

We expand $W(\mathbf{r})$ into SAF's of the crystal system:

$$W(\mathbf{r}) = [\delta(r - r_m)/r^2] \sum_{l\varepsilon} c_{l\varepsilon} P_{l\varepsilon}(\hat{\mathbf{r}}). \qquad (16)$$

Thus, $a(\mathbf{Q})$ is given by

$$a(\mathbf{Q}) = 4\pi f_{X,N}(\mathbf{Q}) \sum_{l\varepsilon} i^l j_l(Qr_m) c_{l\varepsilon} P_{l\varepsilon}(\hat{\mathbf{Q}}), \qquad (17)$$

where the expansion of $\exp(i\mathbf{Q} \cdot \mathbf{r})$ into SAF's and the orthogonality of the SAF's has been used. The $c_{l\varepsilon}$ can be determined from the observed Bragg intensities. From (14) and (17), one obtains the relation between the $g_{\varepsilon\varepsilon'}^l$ and the observed quantities $c_{l\varepsilon}$:

$$c_{l\varepsilon} = [8\pi^2/(2l+1)] \sum_{\varepsilon'} g_{\varepsilon\varepsilon'}^l \overline{\Pi}_{l\varepsilon'}. \qquad (18)$$

Since, for a given l, for the icosahedral group there is only one totally symmetric function $\overline{\Pi}_{l\varepsilon'}$ as long as l is less than 30, the probability function $f(\omega)$ can be expressed approximately in terms of $c_{l\varepsilon}$ with $l < 30$:

$$f(\omega) = \sum_{l\varepsilon\varepsilon'} [(2l+1)/8\pi^2](c_{l\varepsilon}/\overline{\Pi}_{l\varepsilon'}) \mathcal{M}_{\varepsilon\varepsilon'}^l(\omega). \qquad (19)$$

If dynamic disorder is assumed to be present, the probability function $f(\omega)$ is alternatively given by the rotational potential $V(\omega)$ of the C_{60} molecule as a Boltzmann factor:

$$f(\omega) = \exp[-\beta V(\omega)] \Big/ \int \exp[-\beta V(\omega)] \, d\omega, \qquad (20)$$

and so the rotational potential $V(\omega)$ is

$$V(\omega) = -(1/\beta) \ln[f(\omega)] + C, \qquad (21)$$

where

$$C = -(1/\beta) \ln\left[\int \exp[-\beta V(\omega)] \, d\omega\right]. \qquad (22)$$

We have used a formalism similar to (1) – (22) earlier to derive the coefficients in series expansions of the rotation potentials $V(\omega)$ in terms of mixed rotator functions $\mathcal{M}_{\varepsilon\varepsilon'}^l(\omega)$ (Vogt & Prandl, 1983; Gerlach, Prandl & Vogt, 1984; Hoser, Joswig, Prandl & Vogt, 1985). Here we aim directly at the $V(\omega)$ given in (21), which to our knowledge has not yet been applied earlier either for rotational potentials or in particular to the C_{60} case. In applying (21), we avoid difficulties with the high-temperature expansion of Boltzmann factors encountered as soon as the condition $|V(\omega)|/kT \ll 1$ is not obeyed (Lamoen & Michel, 1993).

4. Application to C_{60}

4.1. C_{60} number density

4.1.1. *Maximum-entropy reconstruction*. From diffraction experiments, we obtain a set of unphased structure factors $|F_{obs}^{hkl}| \simeq (I_{obs}^{hkl})^{1/2}$. Owing to the centrosymmetry of the crystal structure with space group

$Fm\bar{3}m$, the phases are 0 or π. Thus, the determination of the phases reduces to the determination of signs ± 1. Using a simple spherical-shell model, *i.e.* the density of the 60 C atoms averaged over a sphere with radius 3.54 Å, we carried out a preliminary phasing of the structure factors. These signs were subsequently coupled to the measured moduli of the structure factors and three-dimensional electron as well as nuclear densities are reconstructed by the maximum-entropy method (MaxEnt). A detailed description of the MaxEnt program we use was given previously (Papoular & Gillon, 1990a,b). Technically, the latter procedure involved a $64 \times 64 \times 64$ discretization of the unit cell and the three-dimensional densities were retrieved as sets of 64 sections at constant z, including a section at $z = 0$ (Figs. 2a, b).
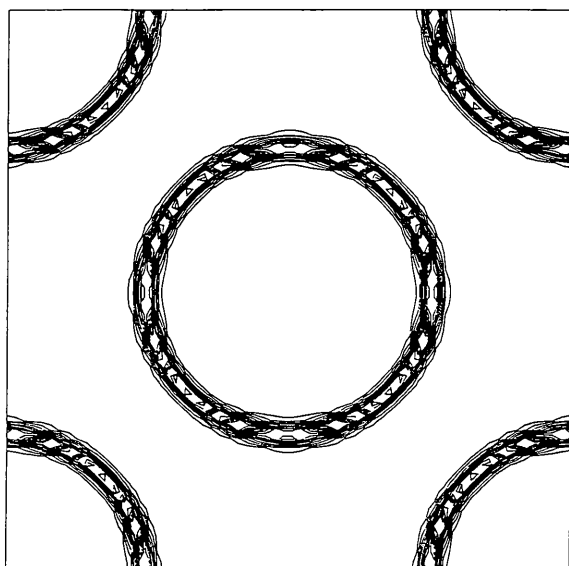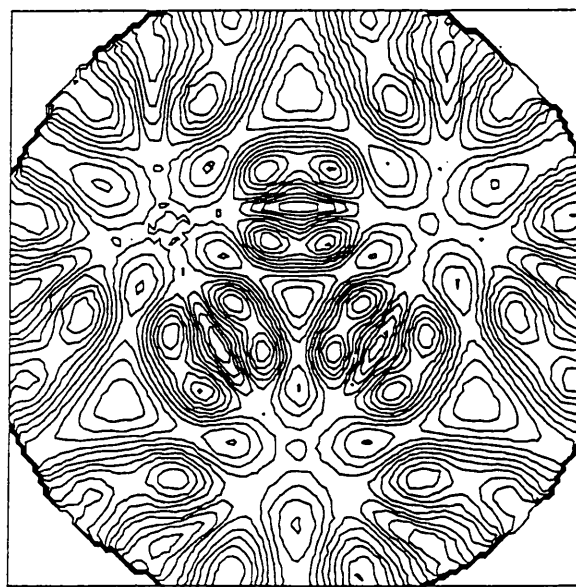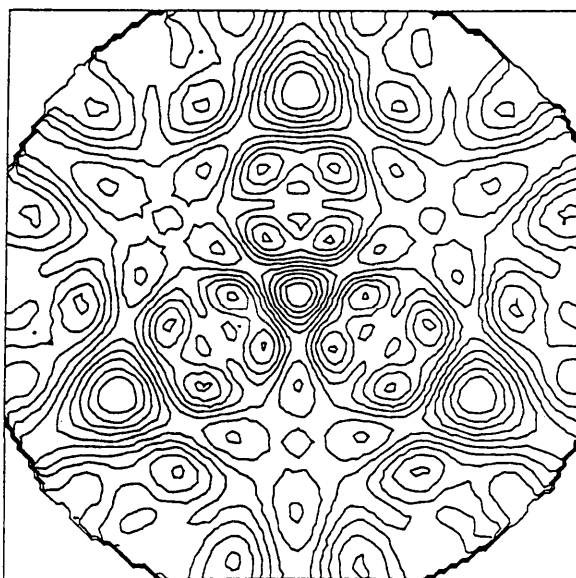

(a)
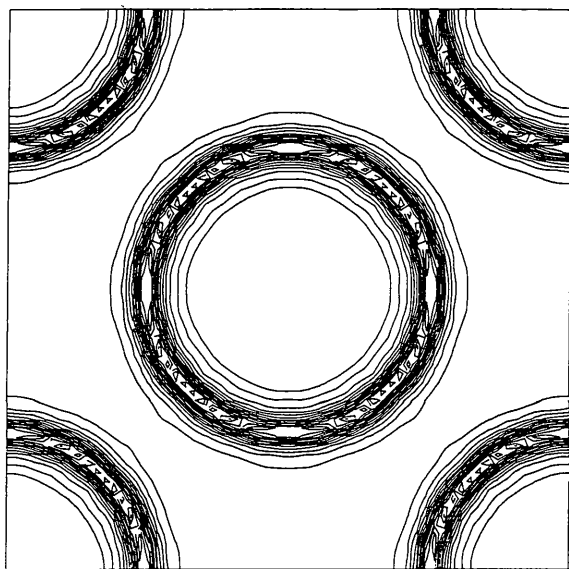
(b)

Fig. 2. (001) section at $z = 0$ through (a) the proton number density and (b) electron density obtained by MaxEnt reconstruction. 15 equidistant level lines between the minimum and maximum densities.

(a)

(b)

Fig. 3. Anisotropic part (stereographic projection) of the radially averaged scattering density for a C_{60} molecule from MaxEnt. (a) Nuclear scattering density. (b) Electron density. Ten equidistant level lines between the minimum and maximum densities. One looks down along [111], [01$\bar{1}$] points to the right and [2$\bar{1}\bar{1}$] downwards.

Table 1. *Results of the refinement with symmetry-adapted functions*

$$R = \frac{\sum_{hkl}||F_o^{hkl}|-|F_c^{hkl}||}{\sum_{hkl}|F_o^{hkl}|}; \quad R_w = \left[\frac{\sum_{hkl}w(|F_o^{hkl}|-|F_c^{hkl}|)^2}{\sum_{hkl}w(F_o^{hkl})^2}\right]^{1/2}.$$

	X-ray	Neutron I	Neutron II
c_{ext}	0.123 (13)	0.0	0.0712 (34)
u (Å^2)	0.0187 (4)	0.0191 (4)	0.0177 (4)
r (Å)	3.5395 (4)	3.5453 (8)	3.5454 (7)
$c_{6,1}$	−0.0180 (11)	−0.0083 (17)	−0.0141 (13)
$c_{10,1}$	0.0132 (13)	0.0104 (20)	0.0143 (18)
$c_{12,1}$	0.0046 (17)	0.0031 (23)	0.0061 (29)
$c_{12,2}$	0.0274 (17)	0.0293 (26)	0.0305 (27)
$c_{16,1}$	−0.0134 (31)	−0.0235 (50)	−0.0089 (57)
$c_{16,2}$	0.0066 (28)	0.0104 (43)	0.0021 (53)
$c_{18,1}$	−0.0025 (25)	0.0011 (49)	0.0062 (73)
$c_{18,2}$	0.0204 (30)	0.0100 (45)	0.0258 (62)
R	0.053	0.048	0.156
R_w	0.018	0.012	0.011
N_{hkl}	205	102	342

Fig. 2 demonstrates that the averaged C_{60} molecules seen by either X-rays or neutrons form very nearly isotropic empty shells, with no evidence for extra density either inside or between them.

In order to compare the results of X-ray and neutron data with the analysis using symmetry-adapted functions, the densities were subsequently interpolated on spheres of selected radii. Different shells with increasing radii were finally added together (Fig. 3). Thus, clear evidence is found for an additional modulation of both nuclear and electron densities and the anisotropy of the radially averaged atomic density of the C_{60} molecules in the high-temperature phase.

4.1.2. Analysis with cubic symmetry-adapted functions (SAF's). Using the method given in §3.2, the measured $|F_{obs}^{hkl}| \simeq (I_{obs}^{hkl})^{1/2}$ are now described by an expansion into cubic symmetry-adapted spherical harmonics (6) and (17). The observed anisotropy of the nuclear- and electron-density distributions is determined by a least-squares fit of the expansion coefficients $c_{l\epsilon}$ with $l > 0$ to the observed $|F_{obs}^{hkl}|$.

Because for the cubic point group $m\bar{3}m$ the number of SAF's for a given l is equal to the number of partitions of l into 6's and 4's, the nonexistence of odd terms in the expansion is easily seen. In addition, if the C_{60} molecule possesses the full icosahedral symmetry, the number of SAF's is given by the number of partitions of l into 6's and 10's (Laporte, 1948). Consequently, $l = 6$ will be the first term common to both sets of SAF's in the expansion followed by $l = 10, 12, 16, 18, \ldots$.

Other adjustable parameters are the radius r of the C_{60} sphere, an isotropic temperature factor U, a scaling factor and c_{ext} to account for secondary extinction according to *SHELXL93* (Sheldrick, 1993).

The refined parameters up to $l = 18$ are given in Table 1. The final R values converged to $R_w^{neutr\ II} = 0.010$ and $R_w^{X\text{-}ray} = 0.018$ for the neutron and X-ray data,

respectively. R values were not significantly improved either by including functions of higher order or by the additional refinement of $l = 4$, 8 and 14 allowed by the cubic site symmetry but forbidden by the icosahedral group of the molecule (Laporte, 1948). For comparison, a refinement of an isotropic carbon sphere, *i.e.* adjusting just the zero-order term in the expansion, leads to poor R values: $R_w^{neutr\ II} = 0.015$ and $R_w^{X\text{-}ray} = 0.037$ for the neutron and X-ray data, respectively.
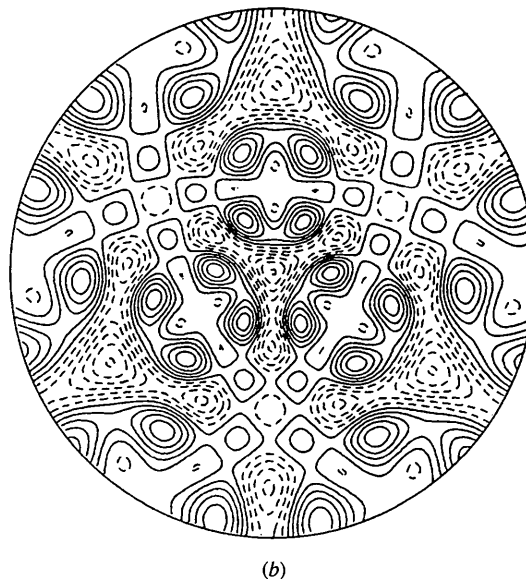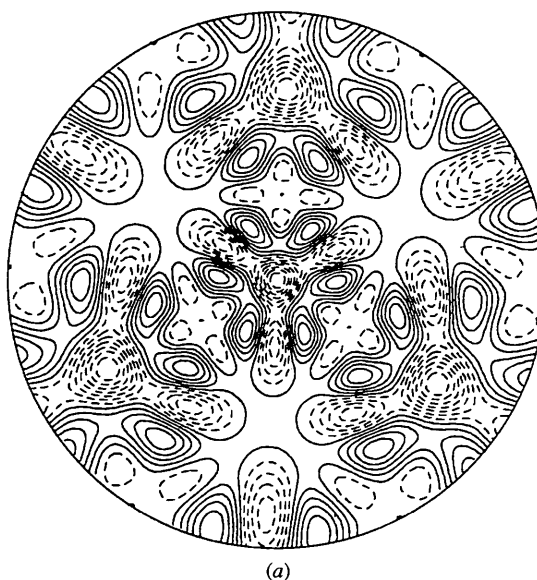

(a)

(b)

Fig. 4. Stereographic projection of the anisotropic part of the modelled (a) nuclear- and (b) electron-density distributions. Level lines are drawn in steps of 2% from the density of an isotropic carbon sphere. Solid level lines correspond to excess density, *i.e.* density greater than the density of an isotropic averaged sphere, dashed level lines to a density deficit. One looks down along [111], [01$\bar{1}$] points to the right and [2$\bar{1}\bar{1}$] downwards.

Fig. 4 shows the anisotropic part of the nuclear- and electron-density distributions in stereographic projections viewed along the [111] direction. 48 maxima are found at polar angles $(\theta, \varphi) = (35.0°, 66.3°)$ and symmetry-related coordinates. They form regular hexagons with an edge length of 1.47 Å around the $\langle 111 \rangle$ directions where the minima in the density distribution are located. The maximum values of the nuclear density exceed the level of the density of an isotropic carbon sphere by 10.1%, whereas the minima only come up to 83.7%. The electron density reflects the nuclear density and no essential differences are found.

4.2. Orientational probability density function

The deviations of the nuclear- and electron-density distributions from the uniform density expected from isotropic rotation clearly demonstrate that some orientations of the C_{60} molecules are more probable than others. But, owing to the very high symmetry, the density distribution does not give any direct hints about the most favourable orientations. The reason becomes immediately evident: the observed number density $W(\mathbf{r})$ is a convolution between the orientational probability density $f(\omega)$ and the molecular number density. Therefore, we attempt to develop the orientational probability density function.

To describe the orientation of the C_{60} molecule in the cubic frame, a set of Euler angles $\omega = (\alpha, \beta, \gamma)$ is used. We take $\omega = 0$ for the molecule oriented with its fivefold axis aligned parallel to the crystal fourfold z axis (Cohan, 1958; Prandl, Schiebel & Wulf, 1996). One of the molecular twofold axes that is perpendicular to this fivefold axis is chosen as the y axis and coincides with another crystal fourfold axis. In this way, the xz plane coincides with one of the molecular mirror planes as well as with a crystal mirror plane. Finally, the x axis is chosen perpendicular to y and z as usual (Fig. 1). In choosing the coordinate system of Fig. 1, we were governed by the argument of mathematical economy
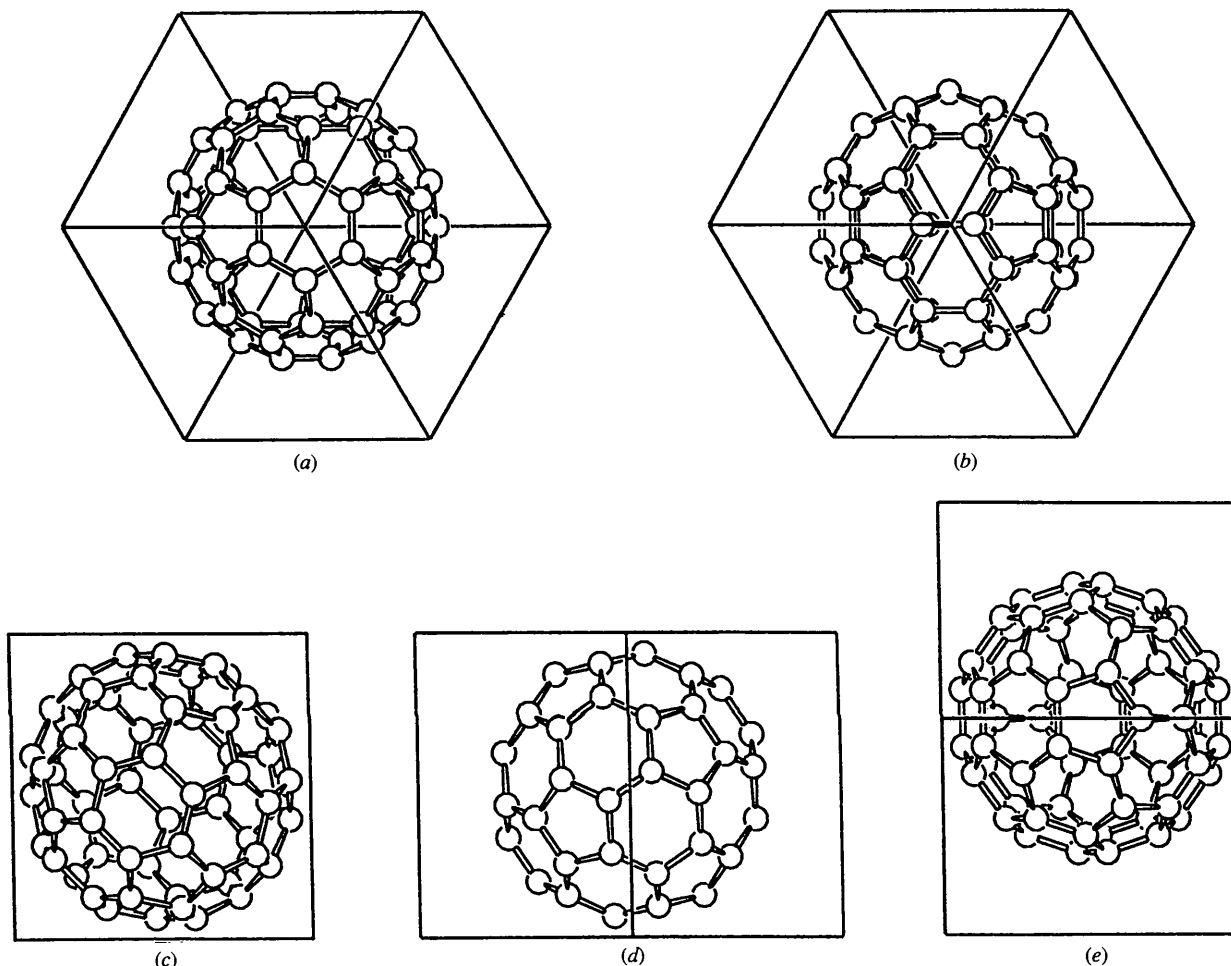

Fig. 5. C_{60} molecule in the orientation ω_1 viewed along different crystal axes. (a) [11$\bar{1}$]; (b) [111], [1$\bar{1}$1], [$\bar{1}$11]; (c) [100], [010], [001]; (d) [110], [101], [011]; (e) [110], [$\bar{1}$01], [01$\bar{1}$].

put forward by Cohan (1958), which was accepted in the general literature on irreducible representation of the icosahedral group, as we discuss in a preceding paper (Prandl, Schiebel & Wulf, 1996). Specifically for C_{60}, a second, mathematically less economic, 'standard orientation' with three mutually perpendicular axes parallel to the cubic x, y, z directions has been introduced (David *et al.*, 1991; Harris & Sachidanandam, 1992). It is clear from general group-theoretical invariance principles that any series representation of physical quantities must have identical coefficients independent of the choice of the coordinate system as long as the principles governing such a symmetry-adapted expansion, namely that the physical objects like number densities or orientational probability densities be described in the same reference system of coordinates, are respected. For the demonstration of experimental results, *e.g.* the dependence of $f(\omega)$ or $V(\omega)$ on the rotation about a molecular axis parallel to a lattice direction (*cf.* Figs. 7–10), one has to apply a rotational algorithm in either case (Altmann, 1986).

With our choice for $\omega = 0$, $f(\omega) = f(\alpha, \beta, \gamma)$ shows fourfold symmetry in α and fivefold symmetry in γ. Consequently, the Euler-angle space may easily be reduced to $0 \le \alpha < 90°$, $0 \le \beta < 180°$, as usual, and $0 \le \gamma < 72°$.

The orientational probability density function is then evaluated according to (19). The molecular constants $\overline{\Pi}_{l,\varepsilon'}$ are calculated from (11) using the bond-length ratio determined by Leclerq *et al.* (1993).

An isotropically rotating C_{60} molecule would adopt every orientation with equal probability, therefore $f(\omega)$ would be constant with $f(\omega) = f^o = 1/8\pi^2 = 0.01267$. The probability density determined, however, shows very well developed maxima, which were found in a 3D search in the Euler-angle space. The main maxima $f^{m1}(\omega_1)$ occur for all data sets at $\omega_1 = (45°, \beta_1, 0°) = (45°, 87.89°, 0°)$. In addition, we find a second, smaller, maximum $f^{m2}(\omega_2)$ at $\omega_2 = (45°, \beta_2, 0°) = (45°, 17.36°, 0°)$. Both types of maximum are found at 240 symmetry-equivalent
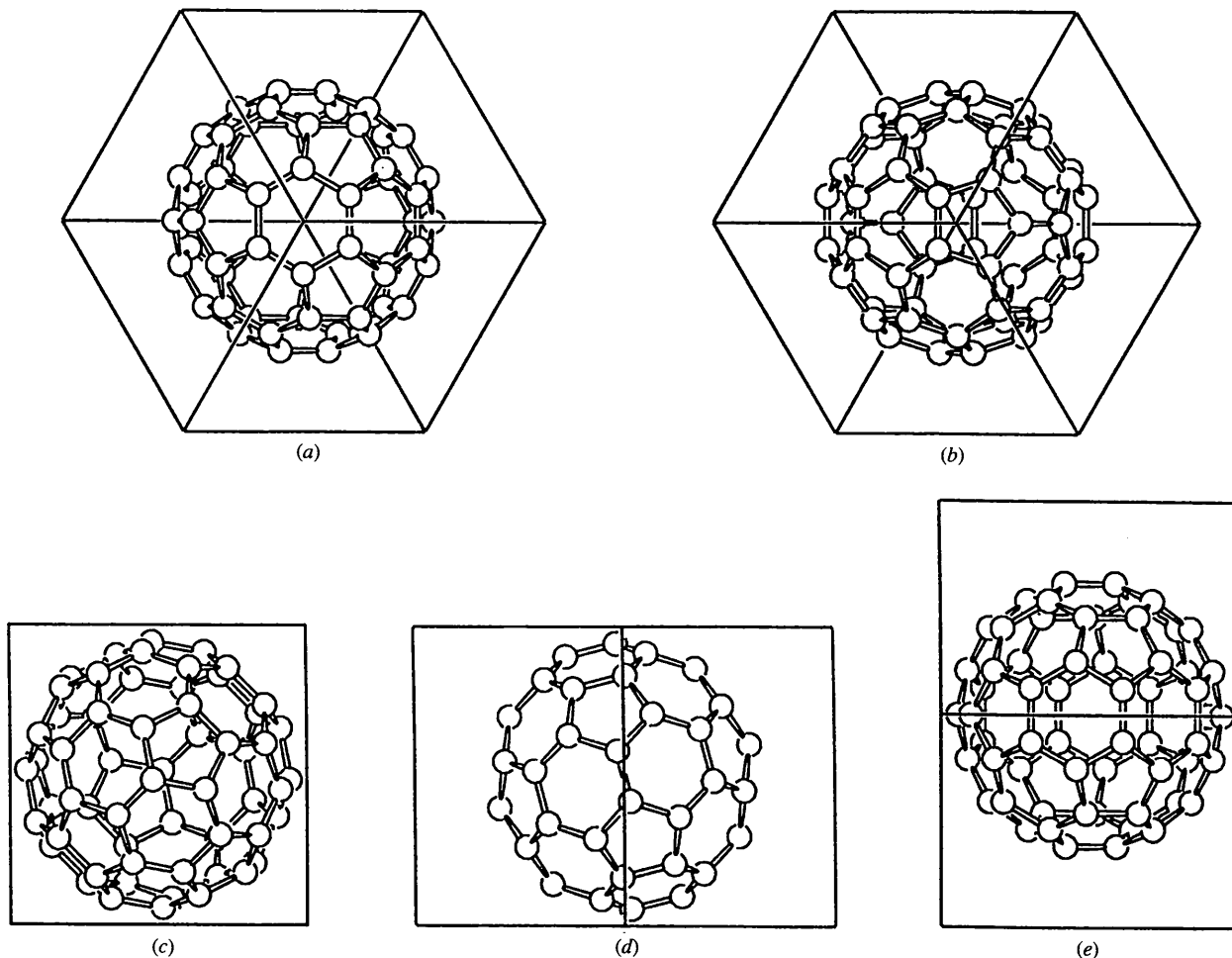

Fig. 6. C_{60} molecule in the orientation ω_2 viewed along different crystal axes. (*a*) [111]; (*b*) [11$\bar{1}$], [1$\bar{1}$1], [$\bar{1}$11]; (*c*) [100], [010], [001]; (*d*) [1$\bar{1}$0], [$\bar{1}$01], [01$\bar{1}$]; (*e*) [110], [101], [011].

Table 2. *Maximum and minimum values of the orientational density distribution function obtained from the X-ray and neutron data*

$$\Delta V = V_{\max} - V_{M_1}; \quad \Delta V_{12} = V(\omega_2) - V(\omega_1).$$

	X-ray	Neutron I	Neutron II
$f(\omega_1)$	0.0390 (12)	0.0374 (20)	0.0383 (20)
$f(\omega_2)$	0.0100 (8)	0.0143 (16)	0.0133 (17)
$f(\omega)_{\min}$	0.0066 (4)	0.0065 (8)	0.0065 (3)
ΔV (K)	525 (20)	516 (38)	522 (20)
ΔV_{12} (K)	383 (27)	283 (35)	313 (41)

points in Euler space. β_1 as well as β_2 are special rotations determined by the condition that a threefold molecular and a threefold crystal axis should coincide. Specifically, we find $\beta_1 = 180° - \alpha_{53} - \alpha_{43}$ and $\beta_2 = \alpha_{43} - \alpha_{53}$, where α_{43} is the angle between a fourfold and a threefold crystalline axis ($\alpha_{43} = 54.74°$) and α_{53} is the angle between a fivefold and a threefold molecular axis $\{\cos \alpha_{53} = [(3 - \tau)/15]^{1/2}(1 + \tau)$ with $\tau = (1/2)(5^{1/2} + 1)\}$.

The absolute values of f^{m1} and f^{m2} for all three data sets are given in Table 2. Figs. 5 and 6 show the C_{60} molecule in the orientation ω_1 and ω_2 viewed along different crystal axes. From the two sets of Euler angles $(45°, \beta_1, 0°)$ and $(45°, \beta_2, 0°)$, it is obvious that the molecular mirror plane that initially coincides with the [111] crystal mirror plane is rotated by 45° to exactly the [110] mirror plane. Simultaneously, the molecular y axis is rotated to the [1$\bar{1}$0] direction. Finally, a rotation around the molecular y axis about $\beta_1 = 87.89°$ nearly moves the fivefold axis to [110] but aligns exactly a molecular and a crystalline threefold axis. A rotation around the molecular y axis about $\beta_2 = 17.36°$ moves a hexagon towards [110] but also results in a molecular and a crystalline threefold axis aligned parallel to each other.

Thus, both orientations are characterized by the coincidence of a maximum number of symmetry elements. The orientation ω_2 may be obtained from ω_1 either by a rotation by 60° around the crystalline threefold axis or, alternatively, by a rotation of 41.81° around a crystalline twofold axis (*cf.* Figs. 5*d* and 6*d*).

To demonstrate the shape of the different maxima, Fig. 7 shows a two-dimensional section through $f(\omega)$ at $\gamma = 0°$. Two of the main maxima M_1 show up as well developed peaks, whereas two of the secondary maxima M_2 are found as lower peaks. The other peaks found in Fig. 7 are due to tangential cuts through main maxima located at $\gamma \neq 0°$. All maxima have a full width at half-maximum of roughly 20°. This is demonstrated in Fig. 8, where a one-dimensional cut through the maxima is drawn.

4.3. *The rotational hindrance potential*

Once the orientational probability density function is evaluated, the rotational hindrance potential is eas-

ily obtained from (21): maxima in $f(\omega)$ correspond to minima in $V(\omega)$ and *vice versa*. Therefore, $V(\omega_1)$ represents an absolute potential minimum and $V(\omega_2)$ a second relative minimum. Fig. 9 shows the hindrance potential corresponding to $f(\omega)$ of Fig. 8. The overall potential height amounts to 522 K, whereas the potential difference between the two sets of potential minima is 313 K.

In Figs. 10(*a*)–(*d*), we show the dependence of $V(\omega)$ on the rotation angle φ for some specific uniaxial rotations of the C_{60} molecules. Fig. 10(*a*) shows $V(\omega) = V(\varphi)$ for a rotation of the molecule around one of its threefold axes if this axis is parallel to the cubic [111] direction, denoted as $R3\|3$. A rotation of $\Delta\varphi = 120°$ moves the molecule from one minimum orientation ω_1 to a symmetry-equivalent one ω_1', whereas a rotation $\Delta\varphi = 60°$ results in the orientation ω_2. Fig. 10(*b*) shows $V(\varphi)$ for a rotation around a molecular twofold axis parallel to the cubic [110] direction $R2\|2$. Starting at the absolute potential minimum, a rotation $\Delta\varphi = 41.81°$ results in the second-order minimum orientation ω_2; after another rotation of $\Delta\varphi = 28.72°$, the next secondary minimum is reached; and, after an additional $\Delta\varphi = 41.81°$, an absolute potential minimum at ω_1' is found again. Fig.
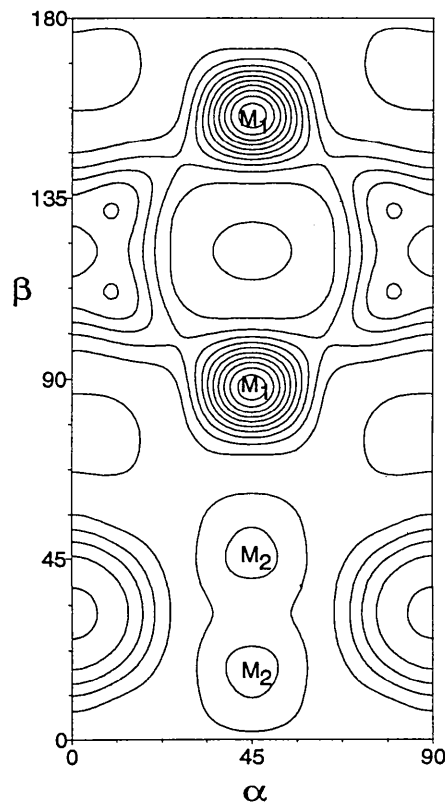

Fig. 7. Two-dimensional section through the orientational probability density function ($0 \leq \alpha \leq 90°, 0 \leq \beta \leq 180°, \gamma = 0°$). The maxima are marked by M_1 and M_2.

10(c) shows the dependence of the potential on $R3\|2$ and on $R5\|2$. The absolute potential minimum is not fully reached with $R5\|2$ but the potential well separating the minima amounts only to 207 K.

Fig. 10(a) may be directly compared with results of a forthcoming paper by Chow, Wochner, Reiter, Moss & Axe (quoted by Axe, Moss & Neumann, 1994) and by Lamoen & Michel (1993), who use a high-temperature approximation of the Boltzmann factor in their analysis of the same experimental data by Chow et al. (1992), since in all three cases $V(\omega)$ is given by the rotation $(R3\|3)$. The only difference is an offset in the rotation angle φ: The standard orientation referred to earlier corresponds in Fig. 10(a) to an angle $\varphi = 120° - \varphi_0$, where $\varphi_0 = 97.76°$ is given by the intrinsic geometry of the Euler-angle space under the action of both the cubic site and the icosahedral molecular point group. Taking this into account, we find $\sin\varphi_0 = \tau(3/8)^{1/2}$ and $\cos\varphi = [(5 - 3\tau)/8]^{1/2}$ with $\tau = (1/2)(5^{1/2} + 1)$. With our choice, the M_1 occur at $n \times 120°$ and the M_2 at $\pm 60°$ from M_1. This means that the locations of the extrema are due to symmetrical properties of the Euler-angle space and not to the numerical size of $V(\omega)$.

We find the secondary minimum M_2 in Fig. 10(a) by $\Delta V_{21} = V_{M_2} - V_{M_1} = 313$ K above the absolute minimum M_1 and the maxima by $\Delta V = V_{max} - V_{M_1} =$

522 K above M_1. Chow et al. (in Axe, Moss & Neumann, 1994) find $\Delta V = 539$ K, which compares well with our finding. The $\Delta V = 800$ K by Lamoen & Michel (1993) is higher, apparently as the result of their approximation. The secondary minimum M_2 is also seen by Lamoen & Michel (1993), whereas it is replaced by a plateau by Chow et al. This latter feature is puzzling, since our Fig. 8 has small maxima at the M_2 positions for Chow's data, which become local minima of $V(\omega)$. Following an erratum to the article by Axe, Moss & Neumann (1994), this discrepancy has been removed very recently: Accordingly, Chow et al., in their forthcoming paper, also find minima M_2 at $\Delta\varphi = \pm 60°$ from M_1 (Fig. 10a).

The potential maxima found are relatively low as compared with the thermal energy of 295 K available to the system. For the actual rotational diffusion of the molecules, one has to take into account that pathways over saddle points with lower activation energy connect the energy minima in $V(\omega)$. Gerling & Hüller (1983) have shown by a molecular dynamics simulation of the rotation of NH_4 that these paths play an essential role in the rotational dynamics if random forces are present.

5. Discussion

The analysis of diffraction data of C_{60} single crystals given in §4.1 clearly demonstrates that the averaged C_{60} molecules seen by either X-rays or neutrons form
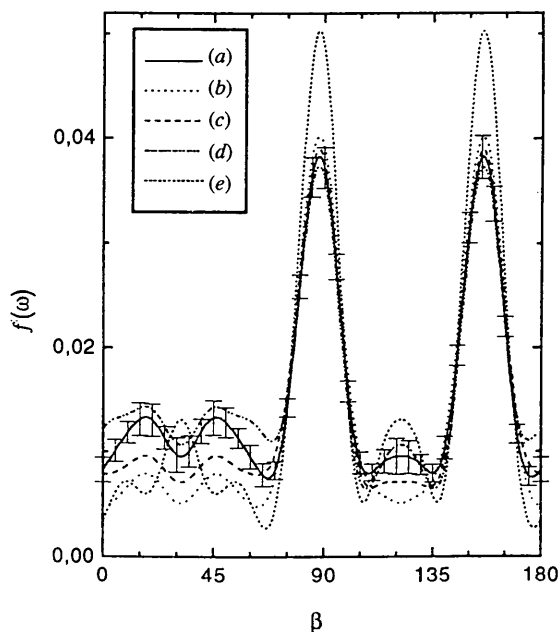

Fig. 8. One-dimensional cut through the orientational density distribution with $\alpha = 45°$ and $\gamma = 0°$. (a) Neutron II with error bars calculated from the standard deviation given in Table 1; (b) neutron I; (c) X-ray (Table 1). For comparison, $f(\omega)$ calculated with the parameter set from (d) Chow et al. (1992) and (e) David et al. (1993) (corrected by a factor $2^{-1/2}$, as pointed out by Michel, Lamoen & David, 1995), is included.
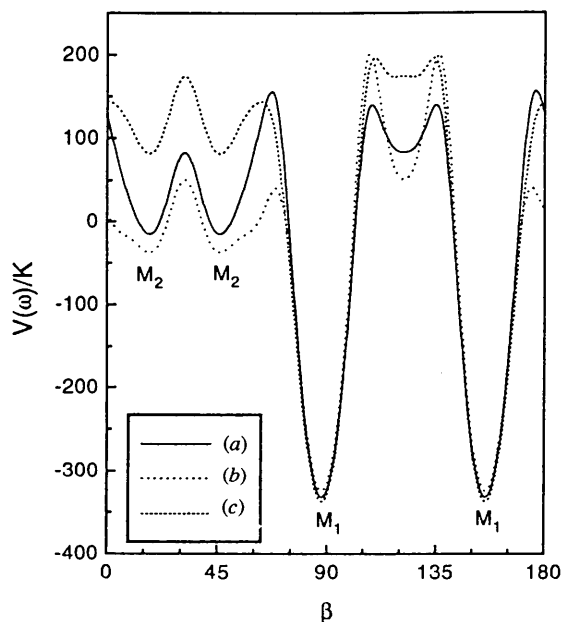

Fig. 9. One-dimensional cut through the rotational hindrance potential calculated from $f(\omega)$ shown in Fig. 8. (a) Neutron II, (b) neutron I, (c) X-ray (Table 1).

very nearly isotropic empty shells, with no evidence for extra density either inside or between them (Fig. 2). Reconstruction of the nuclear- or electron-density distribution by the maximum-entropy method confirms the anisotropy of the averaged density of the C_{60} molecules in the high-temperature phase. For this reconstruction, a quasi model-independent phasing of the measured $|F_{obs}^{hkl}|$ is applied. It turned out in the subsequent refinement

with symmetry-adapted functions that indeed the main contribution to the calculated structure factors comes from the isotropic part in (7) and therefore determines the phases. In fact, our results for the observed density distribution obtained by MaxEnt as well as with the expansion into SAF's are in excellent agreement with each other and with those published by Chow *et al.* (1992) from synchrotron diffraction data. In particu-
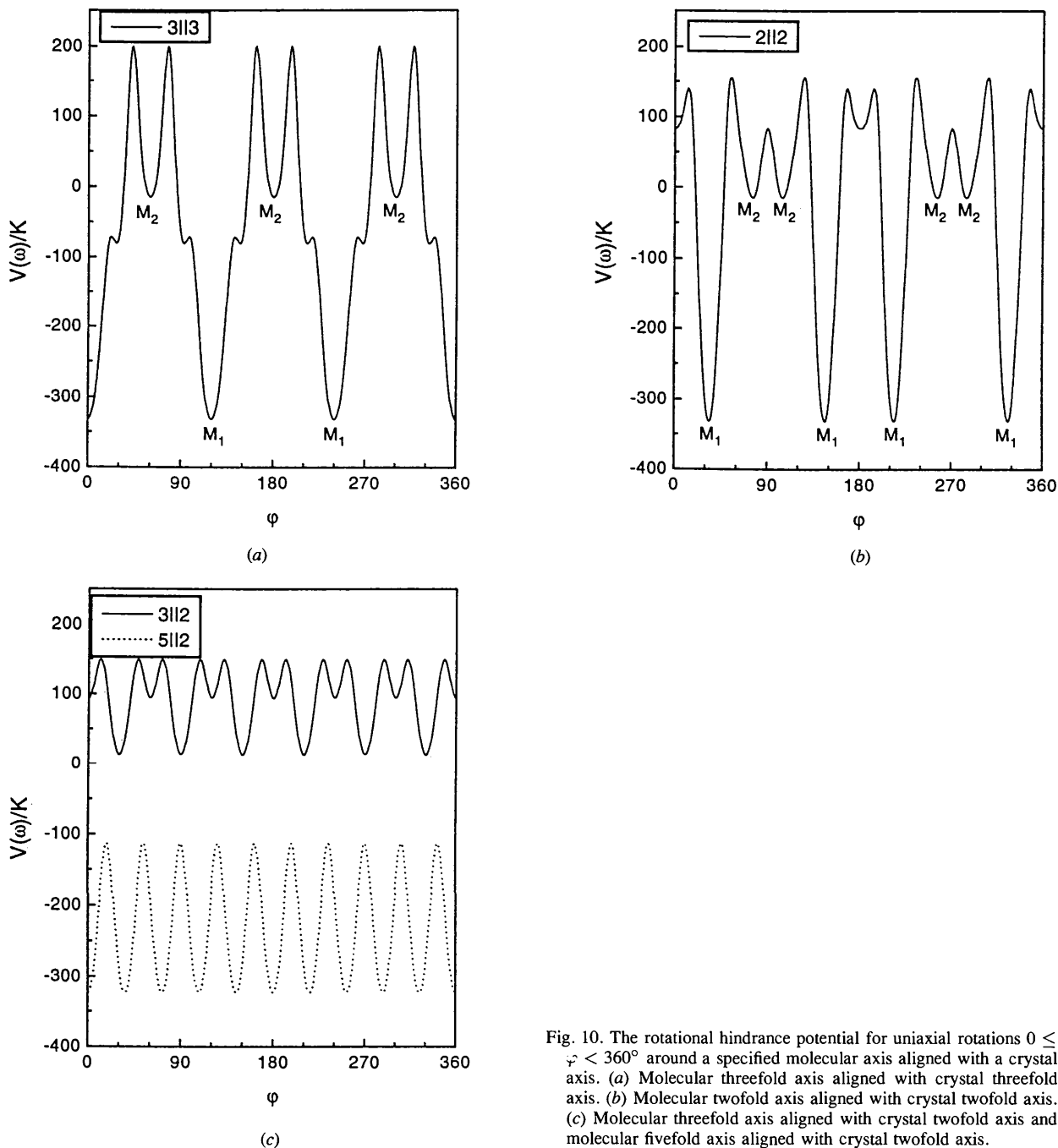

(a)

(b)

(c)

Fig. 10. The rotational hindrance potential for uniaxial rotations $0 \le \varphi < 360°$ around a specified molecular axis aligned with a crystal axis. (a) Molecular threefold axis aligned with crystal threefold axis. (b) Molecular twofold axis aligned with crystal twofold axis. (c) Molecular threefold axis aligned with crystal twofold axis and molecular fivefold axis aligned with crystal twofold axis.

lar, our modelled electron density (Fig. 4b) is nearly identical with Chow et al.'s.

The orientational probability density distribution $f(\omega)$ evaluated in §4.2 shows two different types of maxima at ω_1 and ω_2. From Figs. 5 and 6, it is obvious that these orientations are related to the major and minor orientations found by David, Ibberson & Matsuo (1993). Namely, the orientation ω_1 for which the absolute maximum of $f(\omega_1)$ is found corresponds to the major orientation with a molecular fivefold axis almost parallel to the [110] direction. In addition, the second less-favourable orientation ω_2, established by a relative maximum of $f(\omega)$, corresponds to the minor orientation with a molecular threefold axis almost parallel to the [110] direction.

From our results, a deviation of the molecular fivefold axis from [110] by $2.11°$ is found. This is in good agreement with the $2.2°$ found by Bürgi, Restori & Schwarzenbach (1993) and may be compared with the deviation of $0.05218°$ reported for the low-temperature phase $Pa\bar{3}$ (David, Ibberson & Matsuo, 1993).

From the results given in §4.2, a more classical crystallographic model in terms of atomic coordinates, displacement factors and population parameters may be constructed. Therefore, we calculated two times 60 C-atom positions denoted by $\{M_1\}$ and $\{M_2\}$, which are determined by the radius of the carbon shell $r = 3.54$ Å found in the refinement with SAF and ω_1 and ω_2. We used these atom positions as input for SHELX76 (Sheldrick, 1976). The refined parameters were extinction correction, one isotropic temperature parameter for all C atoms, and occupancies o_1 for the set $\{M_1\}$ and o_2 for the set $\{M_2\}$. The scaling parameter and all atom coordinates are kept fixed. With only four refined parameters, a weighted R value of $R_w^{M_1+M_2} = 0.05$ is reached. For comparison, refinement of just the set $\{M_1\}$ yielded $R_w^{M_1} = 0.10$ and just $\{M_2\}$ yielded $R_w^{M_2} = 0.12$.

Considering the occupancy of the two molecular settings $\{M_1\}$ and $\{M_2\}$, we find $61.11\,(2)\%$ of the molecules in the orientation ω_1 and $38.88\,(1)\%$ in ω_2. This is in agreement with the ratio found in the $Pa\bar{3}$ structure on heating just before the phase transition by David, Ibberson & Matsuo (1993).

This result may also be compared with the structure analysis by Bürgi, Restori & Schwarzenbach (1993), who found 61% of the molecules in the major orientation with hexagons centred on [111], but with the molecular mirror plane rotated by $\pm7.1°$ compared with the crystal mirror plane. They found no evidence for an additional minor orientation. Instead, they stated that the remaining 39% are best described by an isotropic distribution. This difficulty may be attributed to the secondary character of the minimum M_2: unless the search is very close to M_2 (cf. Figs. 9 and 10a,c), the refinement drops into the main minimum and, compared with the set $\{M_1\}$ alone, an additional homogeneous distribution as introduced by Bürgi, Restori & Schwarzenbach (1993) may improve

the residual. In our case, M_2 and therefore the $\{M_2\}$ set was known precisely and therefore the stability of this set was not at stake.

With the above-described SHELX refinement, we reduced the information given by the orientational probability density function $f(\omega)$ to the occupancy of two particular orientations. This means we change from a continuous model to a discrete one by substituting $f(\omega)$ by a set of δ functions. Considering the widths of the determined maxima, a lot of information is lost. We would like to emphasize that any discretization of the densities or the orientational probability densities of an orientationally disordered crystal is a compromise between the dynamic nature and a conventional crystallographic description of the phenomenon.

Details of the underlying dynamics, which leads to the observed proton or electron density, are easily obtained from $f(\omega)$ by a calculation of the orientational hindering potential $V(\omega)$. Maxima in the orientational probability density function correspond to minima in the rotational hindrance potential. With an overall potential barrier height of 522 K, in principle every path that brings the molecule from one minimum orientation to another one is possible. Nevertheless, one may address the question of which way to pass is the easiest one? Therefore, we evaluated the rotational hindrance potential for some uniaxial rotations. As is seen from Fig. 10, $R3\|3$ (rotation of the molecule around a threefold axis aligned parallel to [111]) or $R2\|2$ (twofold axis aligned parallel to [110]) involve the full barrier height, whereas for $R3\|2$ and $R5\|5$ the hindering potential well is rather low. In particular, $R5\|2$ is favourable because it occurs with very low potential values. But none of these uniaxial rotations allows access to all 2×240 minima orientations. In principle, one can distinguish three possible transitions: firstly, a rotation $R(\omega_1 \rightarrow \omega_2)$ that brings the molecule from one of the absolute minima $V(\omega_1)$ to a second-order minimum $V(\omega_2)$, secondly, a rotation $R(\omega_1 \rightarrow \omega_1')$ and, finally, $R(\omega_2 \rightarrow \omega_2')$. From the results mentioned above, it is obvious that $R(\omega_1 \rightarrow \omega_2)$ involves the full potential well, regardless of whether $R3\|3$ or $R2\|2$ are used. $R(\omega_1 \rightarrow \omega_1')$ and $R(\omega_2 \rightarrow \omega_2')$ may be achieved by $R2\|2$ and alternatively by $R3\|2$ or $R5\|2$. The hindering potential for these rotations is even weaker but with $R3\|2$ and $R5\|2$ no change from ω_1 to ω_2 is possible.

Therefore, we conclude that at sufficiently high temperatures the molecules can easily access all observed minimum orientations undergoing three-dimensional rotations. If, however, the temperature is lowered, transitions $R(\omega_1 \rightarrow \omega_2)$ will die out first. As a result, the molecules will be trapped in either ω_1 or ω_2. Because the potential minimum at ω_1 is deeper compared with ω_2, the majority of the molecules is found at ω_1. Nevertheless, all molecules still have the opportunity to move between 240 distinct orientations by a combination of $R2\|2$ and $R5\|2$ or $R2\|2$ and $R3\|2$, respectively. Thus, the rotation axis changes between different $\langle 110 \rangle$ directions.

Finally, on further cooling, the molecules may undergo uniaxial rotations around either their three- or fivefold axes parallel to $\langle 110 \rangle$. Details of the actual pathways chosen by the molecules and allowed by the inertial forces and the available thermal energies can only be given by molecular-dynamics simulations in a realistic rotational potential $V(\omega)$.

References

Altmann, S. L. (1986). *Rotations, Quaternions and Double Groups*, pp. 73–76. Oxford: Clarendon Press.

Axe, J. D., Moss, S. C. & Neumann, D. A. (1994). *Solid State Phys.* **48**, 149–224; erratum sheet in *Solid State Phys.* **48**.

Bradley, C. J. & Cracknell, A. P. (1972). *The Mathematical Theory of Symmetries in Solids*. Oxford: Clarendon Press.

Bürgi, H.-B., Blanc, E., Schwarzenbach, D., Liu, S., Lu, Y. J., Kappes, M. M. & Ibers, J. A. (1992). *Angew. Chem.* **104**, 667–669.

Bürgi, H.-B., Restori, R. & Schwarzenbach, D. (1993). *Acta Cryst.* B**49** 832–838.

Chow, P. C., Jiang, X., Reiter, G., Wochner, P., Moss, S. C., Axe, J. D., Hanson, J. C., McMullan, R. K., Meng, R. L. & Chu, C. W. (1992). *Phys. Rev. Lett.* **69**, 2943–2946.

Cohan, N. V. (1958). *Proc. Cambridge Philos. Soc.* **54**, 28–38.

Copley, J. R. D. & Michel, K. H. (1993). *J. Phys. Condens. Matter*, **5**, 4353–4370.

Copley, J. R. D., Neumann, D. A., Cappelletti, R. L. & Kamitakahara, W. A. (1992). *J. Phys. Chem. Solids*, **53**, 1353–1371.

Copley, J. R. D., Neumann, D. A., Cappelletti, R. L., Kamitakahara, W. A., Prince, E., Coustel, N., McCauley, J. P. Jr, Maliszewskyj, N. C., Fischer, J. E., Smith, A. B. III, Creegan, K. M. & Cox, D. M. (1992) *Physica (Utrecht)*, B**180&181**, 706–708.

David, W. I. F., Ibberson, R. M., Dennis, T. J. S., Hare, J. P. & Prassides, K. (1992*a*). *Europhys. Lett.* **18**, 219–225.

David, W. I. F., Ibberson, R. M., Dennis, T. J. S., Hare, J. P. & Prassides, K. (1992*b*). *Europhys. Lett.* **18**, 735–736.

David, W. I. F., Ibberson, R. M. & Matsuo, T. (1993). *Proc. R. Soc. London Ser. A*, **442**, 129–146.

David, W. I. F., Ibberson, R. M., Matthewman, J. C., Prassides, K., Dennis, T. J. S., Hare, J. P., Kroto, H. W., Taylor, R. & Walton, D. R. M. (1991). *Nature (London)*, **353**, 147–149.

Gerlach, P., Prandl, W. & Vogt, K. (1984). *Mol. Phys.* **52**, 383–397.

Gerling, R. W. & Hüller, A. (1983). *J. Chem. Phys.* **78**, 446–453.

Gugenberger, F., Heid, R., Meingast, C., Adelmann, P., Braun, M., Wühl, H., Haluska, M. & Kuzmany, H. (1992). *Phys. Rev. Lett.* **69**, 3774–3777.

Haluska, M., Kuzmany, H., Vybornov, M., Rogl, P. & Fejdi, P. (1993). *Appl. Phys.* A**56**, 161–167.

Harris, A. B. & Sachidanandam, R. (1992). *Phys. Rev. B*, **46**, 4944–4957.

Heid, R. (1993). *Phys. Rev. B*, **47**, 15912–15922.

Heiney, P. A. (1992). *J. Phys. Chem. Solids*, **53**, 1333–1352.

Heiney, P. A., Fischer, J. E., McGhie, A. R., Romanow, W. J., Denenstein, A. M., McCauley, J. P. Jr, Smith, A. B. & Cox, D. E. (1991). *Phys. Rev. Lett.* **66**, 2911–2914.

Hoser, A., Joswig, W., Prandl, W. & Vogt, K. (1985). *Mol. Phys.* **56**, 853–869.

James, H. M. & Keenan, T. A. (1959). *J. Chem. Phys.* **31**, 12–41.

Johnson, R. D., Yannoni, C. S., Dorn, H. C., Salem, J. R. & Bethune, D. S. (1992). *Science*, **255**, 1235–1238.

Krätschmer, W., Lamb, L. D., Fostiropoulos, K. & Huffman, R. (1990). *Nature (London)*, **347**, 354–358.

Lamoen, D. & Michel, K. H. (1993). *Z. Phys.* B**92**, 323–330.

Lamoen, D. & Michel, K. H. (1994). *J. Chem. Phys.* **101**, 1435–1443.

Laporte, O. (1948). *Z. Naturforsch. Teil A*, **3**, 447–456.

Leclerq, F., Damay, P., Foukani, M., Chieux, P., Bellissent-Funel, M. C., Rassat, A. & Fabre, C. (1993). *Phys. Rev. B*, **48**, 2748–2758.

Michel, K. H. (1992*a*). *Z. Phys.* B**88**, 71–78.

Michel, K. H. (1992*b*). *J. Chem. Phys.* **97**, 5155–5162.

Michel, K. H., Copley, J. R. D. & Neumann, D. A. (1992). *Phys. Rev. Lett.* **68**, 2929–2932.

Michel, K. H., Lamoen, D. & David, W. I. F. (1995). *Acta Cryst.* A**51** 365–374.

Müller, F. M. & Priestley, M. G. (1966). *Phys. Rev.* **148**, 638–643.

Neumann, D. A., Copley, J. R. D., Cappelletti, R. L., Kamitakahara, W. A., Lindstrom, R. M., Creegan, K. M., Cox, D. E., Romanow, W. J., Coustel, N., McCauley, J. P. Jr, Maliszewskyj, N. C., Fischer, J. E. & Smith, A. B. (1991). *Phys. Rev. Lett.* **67**, 3808–3811.

Papoular, R. & Gillon, B. (1990*a*). *Neutron Scattering Data Analysis*, edited by N. Johnson. *Inst. Phys. Conf. Ser.* **107**, 101–116.

Papoular, R. & Gillon, B. (1990*b*). *Europhys. Lett.* **13**, 439–444.

Papoular, R. J., Roth, G., Heger, G., Haluska, M. & Kuzmany, H. (1993). *Electronic Properties of Fullerenes. Springer Series in Solid State Sciences*, No. 117, edited by H. Kuzmany, J. Fink, M. Mehring & S. Roth. Berlin: Springer.

Prandl, W. (1981). *Acta Cryst.* A**37**, 811–818.

Prandl, W., Schiebel, P. & Wulf, K. (1996). *Acta Cryst.* A**52**, 171–175.

Press, W. & Hüller, A. (1973). *Acta Cryst.* A**29**, 252–256.

Sachidanandam, R. & Harris, A. B. (1991). *Phys. Rev. Lett.* **67**, 1467.

Sheldrick, G. M. (1976). *SHELX76. Program for Crystal Structure Determination*. University of Cambridge, England.

Sheldrick, G. M. (1993). *SHELXL93. Program for Crystal Structure Determination*. University of Cambridge, England.

Vogt, K. & Prandl, W. (1983). *Solid State Phys.* **16**, 4753–4768.

Wigner, E. P. (1959). *Group Theory and its Application to the Quantum Mechanics of Atomic Spectra*. New York: Academic Press.